Spin–Orbit Alignment of the β Pictoris Planetary System

Stefan Kraus[1] , Jean-Baptiste Le Bouquin[2] , Alexander Kreplin[1] , Claire L. Davies[1] , Edward Hone[1], John D. Monnier[3] ,
Tyler Gardner[3] , Grant Kennedy[4] , and Sasha Hinkley[1]

[1] School of Physics and Astronomy, Astrophysics Group, University of Exeter, Stocker Road, Exeter EX4 4QL, UK; s.kraus@exeter.ac.uk
[2] Universite d'Grenoble Alpes, CNRS, IPAG, F-38000 Grenoble, France
[3] Department of Astronomy, University of Michigan, 311 West Hall, 1085 South University Ave, Ann Arbor, MI 48109, USA
[4] Department of Physics, University of Warwick, Coventry CV4 7AL, UK

Abstract

A crucial diagnostic that can tell us about processes involved in the formation and dynamical evolution of planetary systems is the angle between the rotation axis of a star and a planet's orbital angular momentum vector ("spin–orbit" alignment or "obliquity"). Here we present the first spin–orbit alignment measurement for a wide-separation exoplanetary system, namely on the directly imaged planet β Pictoris b. We use VLTI/GRAVITY spectro-interferometry with an astrometric accuracy of 1 μas (microarcsecond) in the Brγ photospheric absorption line to measure the photocenter displacement associated with the stellar rotation. Taking inclination constraints from astroseismology into account, we constrain the three-dimensional orientation of the stellar spin axis and find that β Pic b orbits its host star on a prograde orbit. The angular momentum vectors of the stellar photosphere, the planet, and the outer debris disk are well aligned with mutual inclinations $\leqslant 3° \pm 5°$, which indicates that β Pic b formed in a system without significant primordial misalignments. Our results demonstrate the potential of infrared interferometry to measure the spin–orbit alignment for wide-separation planetary systems, probing a highly complementary regime to the parameter space accessible with the Rossiter–McLaughlin effect. If the low obliquity is confirmed by measurements on a larger sample of wide-separation planets, it would lend support to theories that explain the obliquity in Hot Jupiter systems with dynamical scattering and the Kozai–Lidov mechanism.

1. Introduction

Some of the earliest theories about the planet formation process were proposed by Kant & Laplace in the eighteenth century and were based primarily on the observation that the orbits of the solar system planets are well aligned with each other and with the Sun's spin axis. In the solar system the three-dimensional obliquity angle ψ, i.e., the angle between the rotation axis of a star and the orbit angular momentum vector of the planets, is $\psi \lesssim 7°$ (Beck & Giles 2005). For transiting extrasolar planetary systems, the *sky-projected* obliquity angle (β) can be measured with the Rossiter–McLaughlin (RM) effect (Queloz et al. 2000). For the short-period systems where RM measurements are possible, significant misalignments have been found in about a third of the systems (Winn et al. 2010), with values ranging from 0° (indicating a perfectly aligned prograde orbit) to 180° (retrograde orbit, e.g., Hébrard et al. 2011). The sky-projected obliquity angle (β) can then be related to the true obliquity (ψ) distribution, either by measuring the line-of-sight inclination of the stellar rotation axis i_s, for instance using astroseismology (e.g., Wright et al. 2011; Zwintz et al. 2019), or by invoking statistical arguments (e.g., Muñoz & Perets 2018).

Several possible dynamical mechanisms have been proposed to explain the observed spin–orbit misalignments. In one class of theories, the inclination of the planet's orbit is excited through multi-body gravitational interactions, such as planet–planet scattering or interactions with stellar-mass companions (Chatterjee et al. 2008; Valsecchi & Rasio 2014). One appeal of this theory is that Kozai–Lidov oscillations and tidal friction can facilitate both inward migration while increasing simultaneously the obliquity of the planet orbit, thereby explaining key

characteristics of the Hot Jupiter population (Kozai 1962; Fabrycky & Tremaine 2007).

Alternatively, it has been proposed that the stellar rotation axis and orbital angular momentum vector of the planet-forming disk might not be aligned from the start. Misalignments between the stellar rotation axis and disk might be induced by magnetic (Lai et al. 2011) or fluid-dynamical effects (Rogers & Lin 2013). The disk might also be tilted due to turbulent motions in the star-forming cloud (Fielding et al. 2015), due to the complex dynamical interactions in the dense clusters where stars form (Bate et al. 2010), or disk-tearing effects induced by the dynamical interactions in multiple systems (Nixon 2012; Kraus et al. 2020).

In order to distinguish between these scenarios, it is essential to probe the planet obliquity distribution over a wide orbit separation range. One fundamental limitation for obtaining obliquity measurements with the RM effect is that this method can only be applied for transiting systems, i.e., typically for systems with periods of a few days to tens of days.

For wide-separation planets with astrometric orbits, the sky-projected obliquity angle can be derived from spectro-interferometric observations, such as provided by ESO's Very Large Telescope Interferometer (VLTI). This method employs measuring wavelength-differential phases in photospheric absorption lines in order to derive the photocenter shift associated with the stellar rotation. Here, we present VLTI/GRAVITY high spectral resolution data of the β Pictoris system, marking the second time that this technique is applied to a disk-hosting star (following the measurements that indicated good alignment of Fomalhaut's stellar equator with the orbit of its debris disk and dispersing dust cloud; Le

Bouquin et al. 2009; Gaspar & Rieke 2020) and the first time that the obliquity angle is measured for a directly imaged planetary system.

β Pic is a relatively young (age 24 ± 3 Myr; Bell et al. 2015) A6V-type star at a distance of 19.45 ± 0.05 pc (van Leeuwen 2007) and with a mass of $1.85^{+0.03}_{-0.04} M_{\odot}$ (Wang et al. 2016). Defrère et al. (2012) measured the stellar diameter to 0.736 ± 0.019 mas and the projected rotation velocity is $v \sin i = 130$ km s^{-1} (Royer et al. 2007). The system harbors a large-scale debris disk that exhibits a small-scale misalignment between the extended "primary" disk and a "warped" secondary disk in the inner 85 au (Burrows et al. 1995; Mouillet et al. 1997; Currie et al. 2011; Dawson et al. 2011).

The planet β Pic b has been detected with adaptive optics imaging (Lagrange et al. 2009a) and has an orbital period of ~ 20 yr with a semimajor axis of 10.6 ± 0.5 au. It is on a slightly inclined orbit with respect to the primary disk and might be responsible for triggering the warped secondary disk (Lagrange et al. 2012). The orbit is seen with near-edge orientation ($i = 89°.04 \pm 0°.03$, where $90°$ indicates edge-on viewing geometry) and the planet mass has been estimated to $12.8 \pm 2.2 M_{\rm Jup}$ (Fitzgerald et al. 2009; Lagrange et al. 2009b; Wang et al. 2016; Snellen & Brown 2018; Gravity Collaboration et al. 2020). Lagrange et al. (2019) detected the radial velocity signal for a second $\sim 9 M_{\rm Jup}$ planet, β Pic c, on a ~ 1200 day orbit, corresponding to a semimajor axis of ~ 2.7 au.

In Section 2 we describe our observational setup, followed by a presentation of our modeling results (Section 3), a discussion of the implications (Section 4), and our conclusions (Section 5).

2. Observations

We observed β Pic with the GRAVITY instrument (Gravity Collaboration et al. 2017) on seven nights between 2016 September 15 and 2016 October 20. The observations combined the light from the four VLTI 1.8 m auxiliary telescopes. The telescopes were located on stations A0-G1-J3-K0 (2016 September 15, 17, 18, 19), A0-B2-J2-J3 (2016 October 16), and A0-G1-J2-J3 (2016 October 18 and 20), resulting in projected baseline lengths between 22.93 and 132.36 m (Figure 1).

The interferograms cover the K-band with spectral resolution $\lambda/\Delta\lambda = 4000$ and were recorded with detector integration times of 10 s. In total, we recorded 57 exposures of 300 s onsource integration time on β Pic. Interlayed with the observations on the science star, we observed the calibrator star HD 159868.

Wavelength-differential visibilities and phases were extracted using the GRAVITY pipeline (Release 1.2.4, Lapeyrere et al. 2014). In order to increase the signal-to-noise, we averaged the complex visibilities from the 30 individual frames within an exposure. The sky-projected baseline vectors keep changing within the 5 minutes exposures due to Earth rotation (at $\lesssim 0°.2$ minute^{-1}), which could potentially smear the measured astrometric signal. However, based on the maximum measured astrometric displacement of 8 μas (Section 3) we estimate that the astrometric error induced by the averaging is less than 0.1 μas and therefore negligible in our modeling. Furthermore, we note that this effect would only reduce the amplitude of the derived astrometric displacement without biasing the position angles of the derived astrometry vectors,
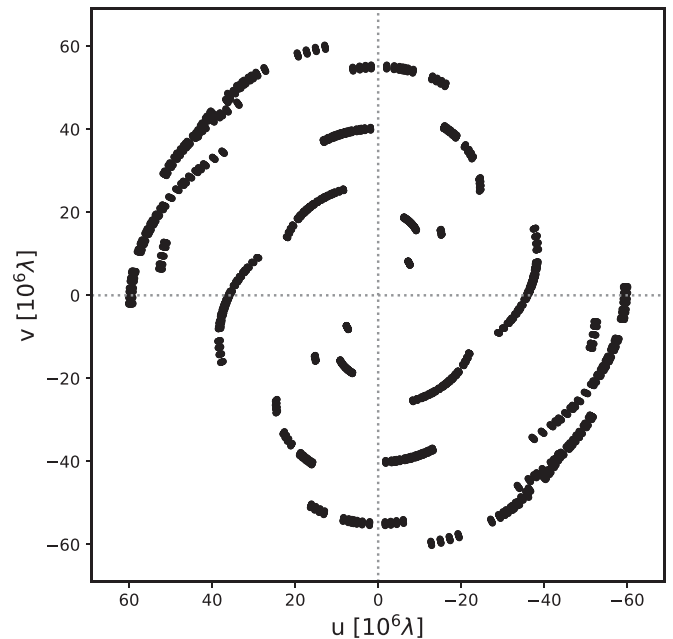

Figure 1. uv-plane of VLTI/GRAVITY observations on β Pic.

even if the averaging would be applied over a longer time interval.

In individual exposures, we achieve a phase rms down to $0°.39$ in the continuum channels near the Brγ 2.1667 μm line. We fit the data from the 57 exposures simultaneously in order to reduce the noise further, resulting in an overall differential astrometric accuracy of 1 μas (as derived from the rms scatter in the continuum channels; gray points in Figure 3, right panel). We reject two observations that exhibit phase rms $>0°.8$ due to poor atmospheric conditions. The spectrum of the pressure-broadened Brγ line is shown in Figure 2 (top panel).
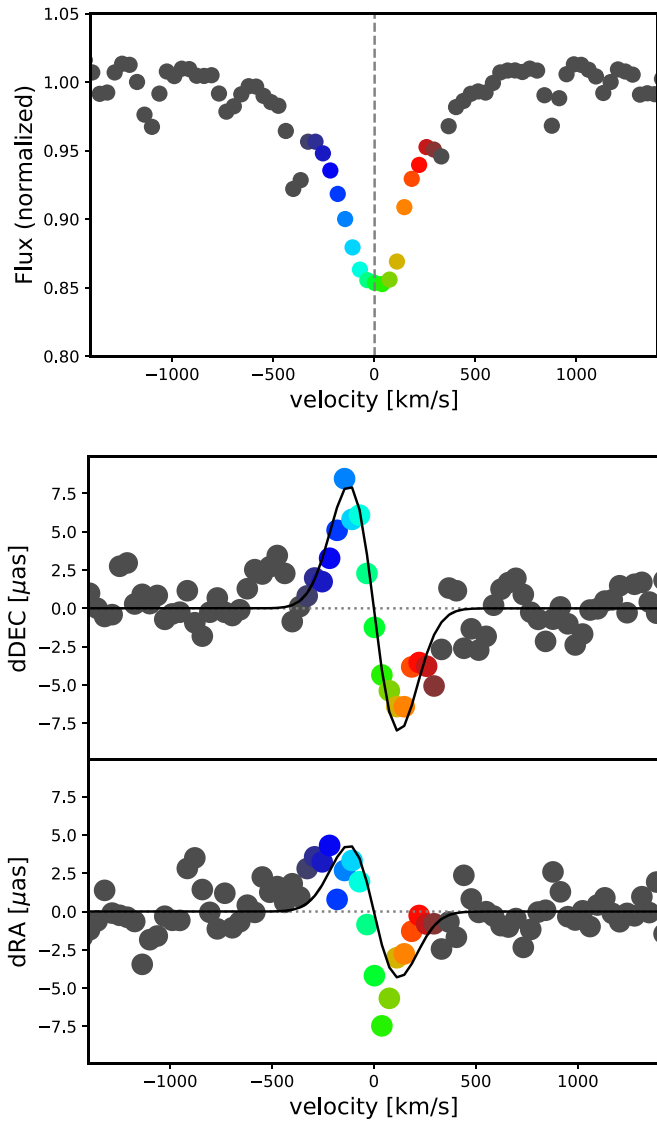
3. Results

We infer the orientation of β Pic's stellar rotation axis from the spatial displacement in the photocenter between the blue-and redshifted wing of the photospheric Brγ absorption line. The photocenter displacement in the line wings with respect to the continuum "center of light" is just ~ 8 μas or $\sim 1/100$th of the stellar diameter, but it can be measured with high significance from our wavelength-differential phases.

The wavelength-differential phase $\phi(\lambda)$ in a given spectral channel, λ, and on a given baseline vector $\boldsymbol{B}$ at projected baseline coordinates (u, v) is given by the equation

$$\phi(\lambda) = \frac{2\pi}{\lambda} \boldsymbol{\mathcal{B}} \cdot \boldsymbol{x}(\lambda), \tag{1}$$

where λ is the wavelength of the considered spectral channel and $\boldsymbol{x}(\lambda)$ the photocenter displacement vector in the channel with respect to the continuum (Le Bouquin et al. 2009).

To maximize the signal-to-noise on the derived photocenter displacement vectors $\boldsymbol{x}(\lambda)$ for a given spectral channel λ, we arrange the n measured differential phases in vector $\phi(\lambda)$ and the corresponding baseline vectors in the $n \times$ two-dimensional matrix B. Using the inverse matrix of B we can rewrite

Figure 2. Spectrum (top panel) and position–velocity diagrams along north–south and east–west directions (bottom panel).

Equation (1) as

$$\boldsymbol{x}(\lambda) = \frac{\lambda}{2\pi} B^{-1} \phi(\lambda)^{\top}. \tag{2}$$

Applying this equation to our data results in the photocenter vectors shown in Figure 3. The R.A. and decl. components of these vectors are also shown as position–velocity diagrams in Figure 2 (bottom). The data show that the photocenter in the blueshifted wing of the Brγ line is displaced to the northeast (Figure 3, right). As the line is in absorption, this indicates that the blueshifted absorption is strongest on the southwestern side of the star, and thus the photocenter shifts to the northeast. Accordingly, the blueshifted (approaching) side of the rotating photosphere is toward the southwest. The phases predicted by the model are overplotted on the measured differential phases in Figure 4.

In order to determine the position angle of the stellar rotation axis quantitatively, we parameterize the wavelength-dependence of the photocenter displacement between the blue- and redshifted line wing with a S-shaped function $S(\lambda) = a(\lambda) \cdot \exp(-a(\lambda)^2)$, where $a(\lambda) = 2(\lambda - \lambda_{\mathrm{Br}\gamma})/w_{\mathrm{Br}\gamma}$,

and $\lambda_{\mathrm{Br}\gamma}$ and $w_{\mathrm{Br}\gamma}$ are the central wavelength and width of the line. This function provides a good approximation for the photocenter displacement due to rotation in a marginally resolved photosphere. We fit this function to the astrometry vectors $\boldsymbol{x}(\lambda)$ in the complex plane:

$$\boldsymbol{x}(\lambda) = c \cdot S(\lambda), \tag{3}$$

where c is a complex number. The phase of c gives the position angle of the spatial displacement between the blue- and redshifted line wings, i.e., the stellar equator is oriented along $\Omega_s = \tan^{-1}(\Re c/\Im c)$. We determine the uncertainties through bootstrapping.

For our data set on β Pic, we derive the sky-projected position angle of the equator to $\Omega_s = 29° \pm 4°$, with the southwestern side of the photosphere approaching the observer.[5] The bottom panel of Figure 2 shows the model function overplotted on the measured astrometric signals.

There are some small residuals between model and data that might indicate a tiny (1–2 μas) offset between the line photocenter and the continuum photocenter to the west (see the redshifted wing in the bottom panel of Figure 2). Such an offset could indicate that the continuum photocenter is slightly shifted with respect to the center of the stellar photosphere, for instance due to stellar surface structures, diffuse disk emission, or a point source within the ~0″.1 field of view. However, the residuals have a low significance and data with higher signal-to-noise and higher angular resolution is needed to investigate this further. Also, future differential phases measurements at higher spectral resolution could derive an independent estimate for the inclination of the photosphere (see the model images of a inclined rotating photosphere in Figure 8 of Kraus et al. 2012) or detect subtle effects in the velocity field, such as related to differential rotation. However, we do not expect these effects to contribute to the residuals in our measurements.

4. Discussion

Together with the inclination estimate of $i_s = 89°.1$ derived from the pulsation frequency spectrum[6] (Zwintz et al. 2019), our measurement of Ω_s defines the full spatial orientation of the stellar rotation axis, enabling a comparison with the spatial orientation of the planetary orbit and of the large-scale debris disk.

The primary disk is likely seen nearly exactly edge-on, while the warped disk is tilted by $+4°.0 \pm 0°.6$ in position angle with respect to the primary disk (Golimowski et al. 2006; Lagrange et al. 2012) and inclined by $6° \pm 1°$ with respect to the line of sight, with the northwestern part of the disk being tipped nearer to Earth (Ahmic et al. 2009, see Figure 3, left and middle panels). In order to compute the mutual inclination between the different planes, we adopt the orbital elements of β Pic b published by Gravity Collaboration et al. (2020), including an orbital inclination $i_p = 89°.04 \pm 0°.03$ and the longitude of the ascending node $\Omega_p = 31°.88 \pm 0°.05$. For the primary disk plane we adopt $\Omega_{d,p} = 29°.3^{+0°.2}_{-0°.3}$ (Lagrange et al. 2012) and $i_{d,p} = 90°.0 \pm 0°.1$ (Ahmic et al. 2009). The warped secondary disk is oriented along $\Omega_{d,s} = 33°.3 \pm 0°.6$ (Lagrange et al.

---

[5] We follow the convention to measure position angles east of north.

[6] The existing astroseismology measurements constrain the inclination value, but provide no information on the hemisphere that faces toward Earth, resulting in a degeneracy between i_s and $180 - i_s$. Due to the near-edge viewing geometry, this degeneracy adds only a small uncertainty that we take into account when computing mutual inclinations.
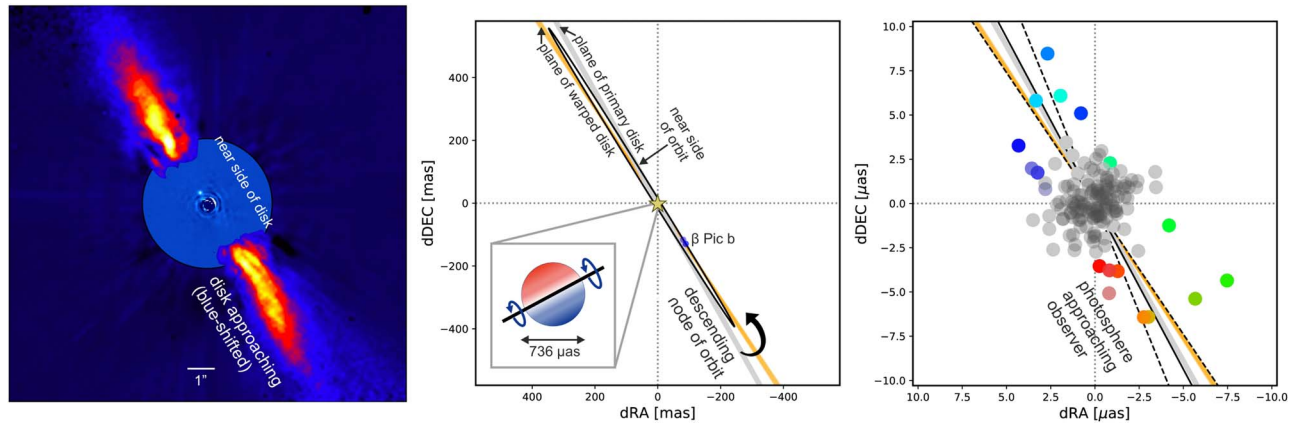
Figure 3. Left panel: scattered light image of β Pic's large-scale debris disk and of β Pic b (credit: ESO; Lagrange et al. 2009a), with the CO blueshifted disk lobe and the side of the disk facing toward the observer indicated. Middle panel: the orbit of β Pic b (orbital elements from Gravity Collaboration et al. 2020), with the plane of the primary disk and the plane of the warped disk marked as gray and orange lines, respectively. The position of β Pic b at the time of our observations has been marked with blue points. Right panel: photocenter displacements measured in the Brγ line (color points) and in the continuum (gray points). The line channels are colored based on their wavelength, using the same color-coding as Figure 2. Given that the line is in *absorption*, the photocenters in the redshifting wing of the line are displaced toward the side of photosphere that is *approaching* the observer (and equivalent for the blueshifted ling wing and the receeding side of the star). The solid black line gives the best-fit position angle for the equatorial plane of the star, with the dashed black lines giving the 1σ error intervals. In all panels, north is top and east is left.

2012), a slight tilt ($i_{d,s} = 84°.0 \pm 1°.0$, Ahmic et al. 2009) that causes the northwestern side of the disk to face toward the observer. This minimal tilt has been deduced from Gemini Planet Imager (GPI) scattered light imaging that show excess scattered light from the northwestern side of the disk, likely due to dust forward scattering (Millar-Blanchaer et al. 2015).

The direction of rotation of the disk has been measured by Dent et al. (2014). They detected a molecular gas clump at a separation at ~85 au that might have been produced by the collision of icy bodies in β Pic's debris belt. The kinematics of the CO clump defines the rotation direction of the disk, with the approaching (blueshifted) line wing to the southwest. Accordingly, the rotation direction deduced from our observations matches the rotation direction for the large-scale disk. It also matches the direction of rotation that has been deduced for β Pic b, indicating that the planet is on a prograde orbit.

The sky-projected orientation of the different planes is shown in Figure 3. The orbital plane of β Pic b is intermediate between the plane of the primary disk (gray line in Figure 3) and of the warp disk (orange line), as already noted by Lagrange et al. (2012).

Our measurements determine the sky-projected obliquity angle to 3° ± 4°. We compute the mutual inclination angle ψ between the angular momentum vectors of the stellar photosphere (s) and the planetary orbit (p) by adopting the equation from Fekel (1981)

$$\cos \psi = \cos i_s \cos i_p + \sin i_s \sin i_p \cos(\Omega_p - \Omega_s), \quad (4)$$

which yields $\psi_p = 3° \pm 5°$ for the planetary orbit. For the primary and secondary disk, the obliquity angles are $\psi_{d,p} = 1° \pm 4°$ and $\psi_{d,s} = 7° \pm 8°$, respectively. This shows that the orbital planes both of the planet and of the primary debris disk are well aligned with the stellar spin, suggesting that the planet formed in a coplanar disk whose angular momentum vector was well aligned with the stellar rotation axis. Any migration to the planet's current location cannot have occurred via mechanisms that would have inflated its mutual inclination.

Our observation provides a first glimpse on the spin–orbit alignment distribution for wide-separation planets, adding new constraints that will help to test hypotheses that have been put forward to explain the origin of the obliquity in short-period planet systems. For the case of β Pic b, we can rule out scenarios that induce stellar obliquities as part of the star formation process or during the disk evolution. The mechanisms that have been proposed to produce such primordial misalignments include planet formation either in a non-coplanar (i.e., warped) disk or in a disk whose angular momentum vector has been shifted with respect to the rotation axis of the star, for instance due to magnetic (Lai et al. 2011) or hydrodynamical effects (Rogers & Lin 2013), or due to turbulence in the cloud that formed the star initially (Bate et al. 2010; Thies et al. 2011; Fielding et al. 2015). A key prediction of these primodial misalignment scenarios is that they can induce obliquities not only for short-separation, but also wide-separation, planets such as β Pic b.

5. Conclusions

We measured the sky-projected obliquity angle for the planet-host star β Pictoris to 3° ± 4°. Incorporating the inclination constraints derived with astroseismology we constrain the three-dimensional orientation of the stellar rotation axis and determine the mutual inclination angle between the angular momentum vector of the star and of β Pic b to 3° ± 5°, indicating that the stellar spin axis is well aligned with the planetary orbit, as well as with the primary disk.

Our finding of spin–orbit alignment for β Pic b suggests that this planet formed in a coplanar disks without primordial misalignments. This is in contrast to theories that describe the occurrence of obliquities as a natural by-product of the star formation process, for instance through turbulent motions in the star-forming cloud (Fielding et al. 2015) or magnetic (Lai et al. 2011) and fluid-dynamical effects (Rogers & Lin 2013) during disk formation. In case our finding of a well-aligned system is representative for wide-separation planets, it would suggest that the population of Hot Jupiters on oblique orbits (found in RM survey at orbit separations between ~0.02 and
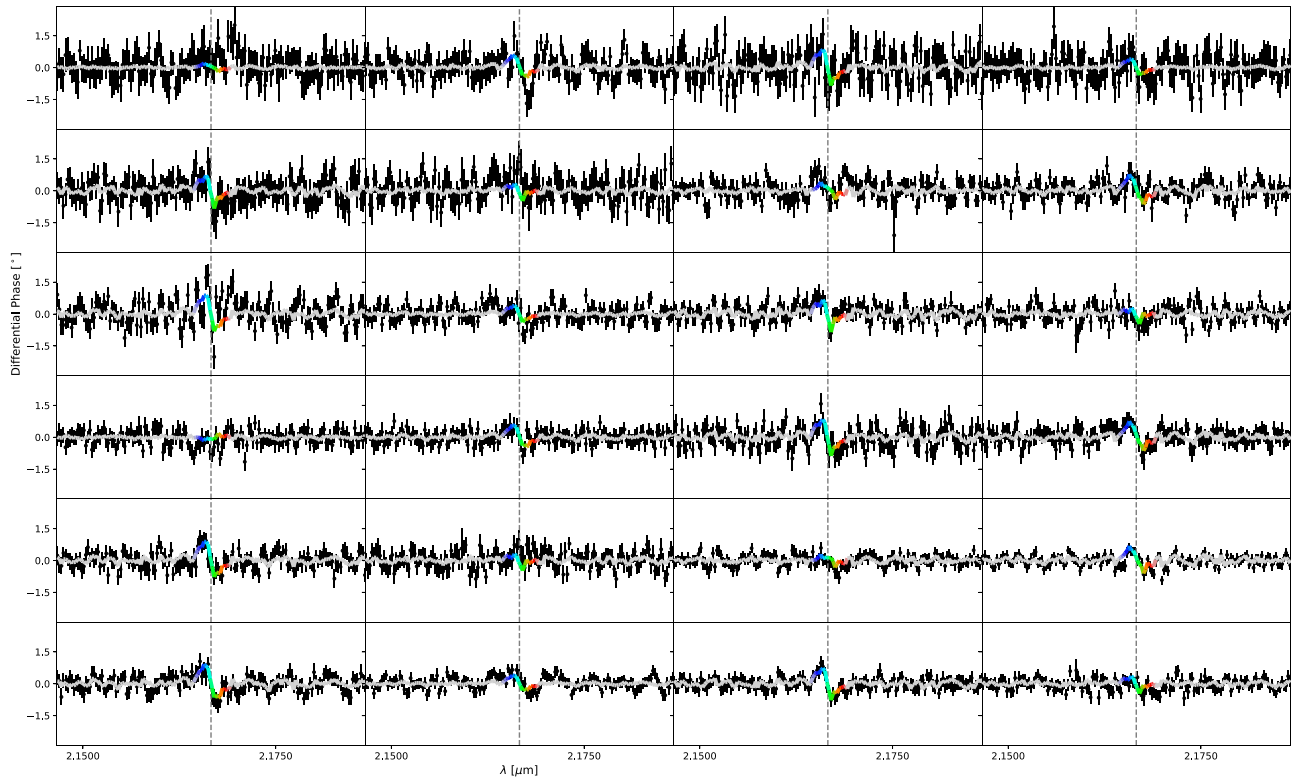
Figure 4. Measured differential phases (points), overplotted with the model phases that correspond to our best-fit photocenter model (line). Each panel shows the measured phases for one of the six baselines, averaged over the full data recording sequence.

0.3 au) are likely transferred to oblique orbits through dynamical processes post-formation. Possible mechanisms include planet–planet scattering, stellar flybys, or the Kozai–Lidov mechanism, where a wide companion orbiting a close binary on a highly inclined orbit can induce oscillations in inclination/eccentricity of the close pair (e.g., Fabrycky & Tremaine 2007).

Observations on a larger sample of planet-hosting stars will be critical to test this hypothesis and to extend the obliquity distribution presently covered by RM-based surveys ($\lesssim$0.3 au) out to planets with orbital separations at tens or hundreds of au. For such wide-separation systems, infrared interferometry at high spectral dispersion provides the only technique to measure the sky-projected obliquity angle. At present, spin–orbit alignment measurements with VLTI are limited to nearby stars with large apparent diameters and to pressure-broadened lines of relatively fast-rotating stars, which strongly limits the numbers of stars that are accessible with this technique. A dedicated high spectral resolution ($R = 25,000$), short-wavelength instrument operating in the J-band (1–1.4 μm) and optimized for precision phase measurements, such as the proposed VLTI visitor instrument BIFROST (Kraus 2019), will be able to mitigate these limitations and enable spin–orbit measurements for hundreds of systems in the planet samples that are expected from direct-imaging facilities (James Webb Space Telescope and Extremely Large Telescopes) and the GAIA astrometry mission. Modeling the obliquity distribution that will be provided by such next-generation instruments will allow testing of the theories that have been put forward to explain the origin of planet obliquity on a statistically significant sample, offering direct insights on the planet formation process and the dynamical evolution that shapes the architecture of planetary systems.

Facility: VLTI.

ORCID iDs

Stefan Kraus ⬤ https://orcid.org/0000-0001-6017-8773
Jean-Baptiste Le Bouquin ⬤ https://orcid.org/0000-0002-0493-4674
Alexander Kreplin ⬤ https://orcid.org/0000-0002-0911-9505
Claire L. Davies ⬤ https://orcid.org/0000-0001-9764-2357
John D. Monnier ⬤ https://orcid.org/0000-0002-3380-3307
Tyler Gardner ⬤ https://orcid.org/0000-0002-3003-3183
Grant Kennedy ⬤ https://orcid.org/0000-0001-6831-7547
Sasha Hinkley ⬤ https://orcid.org/0000-0001-8074-2562

References

Ahmic, M., Croll, B., & Artymowicz, P. 2009, ApJ, 705, 529
Bate, M. R., Lodato, G., & Pringle, J. E. 2010, MNRAS, 401, 1505
Beck, J. G., & Giles, P. 2005, ApJL, 621, L153

Bell, C. P. M., Mamajek, E. E., & Naylor, T. 2015, MNRAS, 454, 593
Burrows, C. J., Krist, J. E., Stapelfeldt, K. R. & WFPC2 Investigation Definition Team 1995, BAAS, 27, 1329
Chatterjee, S., Ford, E. B., Matsumura, S., & Rasio, F. A. 2008, ApJ, 686, 580
Currie, T., Thalmann, C., Matsumura, S., et al. 2011, ApJL, 736, L33
Dawson, R. I., Murray-Clay, R. A., & Fabrycky, D. C. 2011, ApJL, 743, L17
Defrère, D., Lebreton, J., Le Bouquin, J.-B., et al. 2012, A&A, 546, L9
Dent, W. R. F., Wyatt, M. C., Roberge, A., et al. 2014, Sci, 343, 1490
Fabrycky, D., & Tremaine, S. 2007, ApJ, 669, 1298
Fekel, F. C. J. 1981, ApJ, 246, 879
Fielding, D. B., McKee, C. F., Socrates, A., Cunningham, A. J., & Klein, R. I. 2015, MNRAS, 450, 3306
Fitzgerald, M. P., Kalas, P. G., & Graham, J. R. 2009, ApJL, 706, L41
Gaspar, A., & Rieke, G. 2020, PNAS, 117, 9712
Golimowski, D. A., Ardila, D. R., Krist, J. E., et al. 2006, AJ, 131, 3109
Gravity Collaboration, Abuter, R., Accardo, M., et al. 2017, A&A, 602, A94
Gravity Collaboration et al., Nowak, M., & Lacour, S. 2020, A&A, 633, A110
Hébrard, G., Ehrenreich, D., Bouchy, F., et al. 2011, A&A, 527, L11
Kozai, Y. 1962, AJ, 67, 591
Kraus, S. 2019, Proc. The Very Large Telescope in 2030 (Garching: ESO), 36
Kraus, S., Monnier, J. D., Che, X., et al. 2012, ApJ, 744, 19
Kraus, S., Kreplin, A., Young, A. K., et al. 2020, arXiv:2004.01204
Lagrange, A. M., Gratadour, D., Chauvin, G., et al. 2009a, A&A, 493, L21
Lagrange, A. M., Kasper, M., Boccaletti, A., et al. 2009b, A&A, 506, 927
Lagrange, A. M., Boccaletti, A., Milli, J., et al. 2012, A&A, 542, A40
Lagrange, A.-M., Meunier, N., Rubini, P., et al. 2019, NatAs, 3, 1135
Lai, D., Foucart, F., & Lin, D. N. C. 2011, MNRAS, 412, 2790
Lapeyrere, V., Kervella, P., Lacour, S., et al. 2014, Proc. SPIE, 9146, 91462D
Le Bouquin, J.-B., Absil, O., Benisty, M., et al. 2009, A&A, 498, L41
Millar-Blanchaer, M. A., Graham, J. R., Pueyo, L., et al. 2015, ApJ, 811, 18
Mouillet, D., Larwood, J. D., Papaloizou, J. C. B., & Lagrange, A. M. 1997, MNRAS, 292, 896
Muñoz, D. J., & Perets, H. B. 2018, AJ, 156, 253
Nixon, C. J. 2012, MNRAS, 423, 2597
Queloz, D., Eggenberger, A., Mayor, M., et al. 2000, A&A, 359, L13
Rogers, T. M., & Lin, D. N. C. 2013, ApJL, 769, L10
Royer, F., Zorec, J., & Gómez, A. E. 2007, A&A, 463, 671
Snellen, I. A. G., & Brown, A. G. A. 2018, NatAs, 2, 883
Thies, I., Kroupa, P., Goodwin, S. P., Stamatellos, D., & Whitworth, A. P. 2011, MNRAS, 417, 1817
Valsecchi, F., & Rasio, F. A. 2014, ApJ, 786, 102
van Leeuwen, F. 2007, A&A, 474, 653
Wang, J. J., Graham, J. R., Pueyo, L., et al. 2016, AJ, 152, 97
Winn, J. N., Fabrycky, D., Albrecht, S., & Johnson, J. A. 2010, ApJL, 718, L145
Wright, D. J., Chené, A.-N., De Cat, P., et al. 2011, ApJL, 728, L20
Zwintz, K., Reese, D. R., Neiner, C., et al. 2019, A&A, 627, A28